

Machine Learning Prediction of DNA Charge Transport

Roman Korol and Dvira Segal¹

Department of Chemistry and Centre for Quantum Information and Quantum Control, University of Toronto, 80 Saint George St., Toronto, Ontario, Canada M5S 3H6 ^{a)}

(Dated: 28 January 2022)

First principle calculations of charge transfer in DNA molecules are computationally expensive given that charge carriers migrate in interaction with intra- and inter-molecular atomic motion. Screening sequences, e.g. to identify excellent electrical conductors is challenging even when adopting coarse-grained models and effective computational schemes that do not explicitly describe atomic dynamics. In this work, we present a machine learning (ML) model that allows the inexpensive prediction of the electrical conductance of millions of *long* double-stranded DNA (dsDNA) sequences, reducing computational costs by orders of magnitude. The algorithm is trained on *short* DNA nanojunctions with $n = 3 - 7$ base pairs. The electrical conductance of the training set is computed with a quantum scattering method, which captures charge-nuclei scattering processes. We demonstrate that the ML method accurately predicts the electrical conductance of varied dsDNA junctions tracing different transport mechanisms: coherent (short-range) quantum tunneling, on-resonance (ballistic) transport, and incoherent site-to-site hopping. Furthermore, the ML approach supports physical observations that clusters of nucleotides regulate DNA transport behavior. The input features tested in this work could be used in other ML studies of charge transport in complex polymers, in the search for promising electronic and thermoelectric materials.

Keywords: DNA, electrical conductance, charge transport, artificial neural networks

I. INTRODUCTION

Charge migration in DNA is a topic of significant interest with applications to biology, chemistry, physics and engineering¹. First and foremost, both oxidative DNA damage, leading to cancerous mutations^{2,3}, and repair signaling⁴ take place through long-range electron transfer. Beyond its biological function, DNA is an attractive material in nanotechnology given its molecular recognition properties, self-assembly, and structural flexibility⁵. For example, self assembled monolayers of DNA can serve as biosensors for detecting mutated genes⁶, and DNA templates can direct the assembly of nanostructures of desired shapes^{5,7}. Moreover, given its rich electronic properties and automated synthesis, DNA molecules may be used as the conducting material in molecular electronic circuits⁸⁻¹⁰.

Experiments have demonstrated diverse charge transport behavior through DNA. Very long DNA molecules with hundreds of base-pairs (bp) may act like metals, semiconductors, and even insulators¹⁰. Measurements of shorter (5-20 bp) DNA duplexes revealed a broad range of trends: Depending on the base sequence¹¹⁻¹⁴, molecular length^{11,15-18}, backbone composition¹⁹, surrounding environment²⁰, temperature, helical conformation²¹ linkers to the electrodes^{19,22,23} and gating²⁴, DNA charge transport may occur via different mechanisms: deep tunneling^{11,18}, thermally activated hopping^{11,17,18}, resonant ballistic or flickering resonance^{25,26}, and intermediate coherent-incoherent behavior²⁷⁻³⁰.

Calculations of DNA charge transfer are exceptionally challenging given the complexity of the system, with

charge carriers interacting with moving nuclei of the base pairs, backbone, counterions, solvent. Screening DNA sequences to identify excellent or poor conductors and classify transport mechanisms is challenging even when adopting coarse-grained models and computational schemes that only approximately describe atomic dynamics. The elementary components of DNA are four nucleotides forming double-stranded helix DNA (dsDNA). The strands are hybridized by obeying the base-pairing rules: adenine (A) with thymine (T), cytosine (C) with guanine (G). Since the sequence space grows exponentially fast, brute-force all-sequence calculations of charge transport in DNA become essentially implausible for chains with $n \gtrsim 8$ base pairs.

The objective of the present work is to test a machine learning (ML) model for DNA charge transport so as to bypass computational limitations of direct comprehensive calculations. The model predicts the conductance of millions of long metal-molecule-metal DNA junctions based on conductance data of thousands of short (3-7 bp) sequences. Our goal is to use the ML method to provide reasonable numbers for DNA electrical conductance and furthermore predict correct qualitative transport trends for special classes of molecules—in accord with physical considerations. For example, short DNA with an AT block should act as a tunneling barrier with the conductance dropping exponentially with length. In contrast, GC-rich molecules are expected to behave as ohmic conductors with the resistance growing linearly with the number of base pairs¹⁸. Conductance values in DNA molecules extend over many orders of magnitude, with metallic to insulating sequences. The ML model should capture this extreme variability.

The physical setup under consideration is depicted in Fig. 1: A dsDNA molecule with n base pairs is

^{a)}Electronic mail: dvira.segal@utoronto.ca

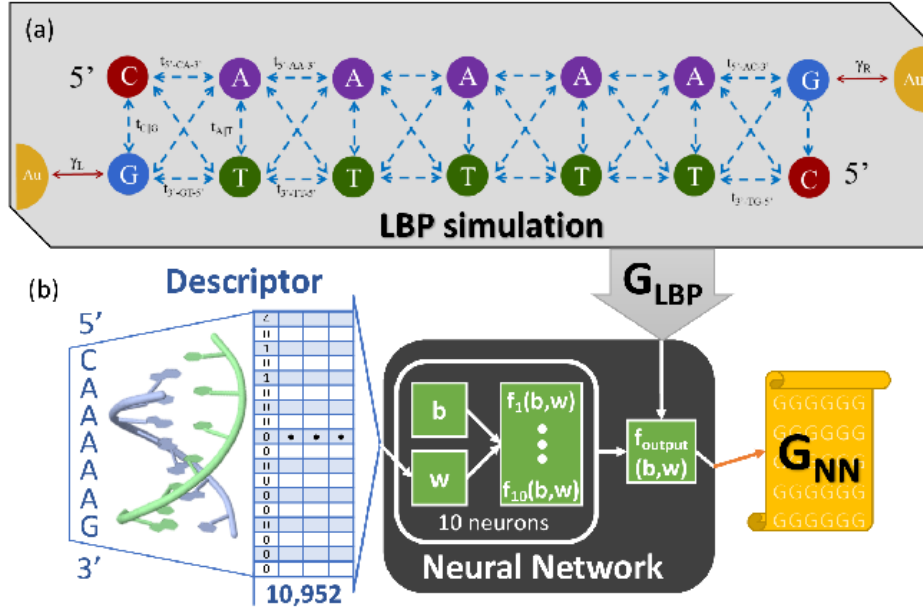


FIG. 1: Machine learning calculation of the electrical conductance of dsDNA junctions. (a) A coarse grained model of a dsDNA junction, depicting the $n = 7$ bp sequence 5'CAAAAAG3'. Sequences are labeled from the 5' to the 3' end. The electronic Hamiltonian is described with a tight binding model; double arrows represent electronic tunneling elements within and in between strands. The effect of the nuclear degrees of freedom is taken into account using a quantum scattering approach, the LBP method. The output of an LBP calculation is the electrical conductance G_{LBP} . (b) The neural network is trained based on the conductances of 10,592 sequences $n = 3 - 7$ bp long. The descriptor exemplified here has 16+2 entries: It counts the occurrence of each of the 16 possible pairs of nucleotides in a single strand in alphabetical order. The sequence 5'CAAAAAG3' depicted here has four pairs of AA (first entry), a single AG pair (third entry), and a single CA pair (fifth entry). The last two entries of the input (0 here) identify the base that is connected to the metals, G,A,T or C, taking the values 0,1,2 or 3, respectively.

connected to metal electrodes at its 3' ends. Assuming molecules are coupled symmetrically to two identical metals, there are 8192 distinct junctions for e.g. molecules with $n = 7$ bp³¹. The conductance of these junctions (as well as of shorter systems) was computed and analyzed in our recent study, Ref.³¹ based on a quantum scattering technique, the Landauer-Büttiker's probe (LBP) method^{32,33}. Here we use this dataset to train a ML model so as to compute the conductance of arbitrarily long DNA junctions. To make the model transferable to sequences of different size, we prepare input features (descriptors) that do not rightly announce on the base sequence itself, but report on molecular composition and the occurrence of local clusters.

We train the ML model on the conductance of 3 to 7 bp sequences. We test it against short molecules in this set, then use it for predicting the behavior of longer molecules up to 18 bp. The quality of predictions is assessed against LBP calculations. Our finding are that the ML model correctly predicts both global features of the ensemble of

molecules, and the behavior of special sequences. Specifically, the model traces the transition from fully coherent (deep tunneling) to ballistic (on-resonance) transfer for stacked A-sequences, the tunneling to hopping crossover in sequences with an AT block, and (with mixed success) hopping conduction in alternating GC-sequences. These results demonstrate that ML models can provide a cheap assessment of quantum dynamics and transport in complex systems.

The paper is organized as follows. In Sec. II we discuss the Landauer-Büttiker probe method and present the machine learning framework. In Sec. III we illustrate the performance of our neural networks for short sequences, as well as the extrapolation onto longer sequences. We further demonstrate that when used appropriately, the neural networks can learn the mechanism of conduction and accurately predict the conductance of molecules that are significantly longer than sequences in the training set. We conclude in Sec. IV.

II. METHODS

A. Physical setup

Loosely speaking, we classify DNA charge transport as ‘short’ or ‘long’ if it extends at most 2 nm ($n < 7$ bp), or up to 10 nm ($7 < n < 30$ bp), respectively; recall that the distance between base pairs of DNA is approximately 3.4 Angstroms. Ultra long molecules extend beyond 10 nm, and are not examined in this study, though our approach is applicable to arbitrary length. Single-molecule conductance experiments in a metal-molecule-metal geometry typically employ DNA molecules in the range of $7 < n < 20$ ^{11,18,19,21,24,28}. In contrast, DNA electrochemistry experiments on monolayers probe transport in molecules with as many as 100 bp, see e.g. Ref.²⁶.

The prototype molecular junction under consideration is depicted in Fig. 1(a). A single dsDNA molecule with n base pairs is connected to metal electrodes at its 3’ ends. While we sketch the DNA as if it directly attaches to the metals, in fact in e.g. break junction experiments the molecule is modified with linkers (thiols, amines) to ensure sufficiently strong chemical binding of the molecule to the electrodes. The overall-effective coupling energy of the nucleotide at the interface to the metal is captured by the hybridization parameters γ_L and γ_R . Nuclear degrees of freedom are not pictured in Fig. 1. Implementing their effect on charge conduction is explained in the next section.

B. Landauer Büttiker probe simulations

Charge migration in dsDNA takes place inside the double helix along the π stacking. To preserve its structure thus conductive properties, dsDNA must be maintained in a buffered solution, making it a highly flexible material with nuclear dynamics of the nucleobase, reorganization of solvent molecules and counterions, and displacements of structural elements. The timescales of these processes range from picoseconds to milliseconds.

Simulations of charge carrier dynamics in DNA must therefore take into account the impact of atomic motion on charge conduction. Ab-initio techniques are impractical to treat this problem, and even hybrid methods are challenging: Explicit atomistic calculations at the level of molecular dynamics (for sampling configurations), combined with quantum mechanics/molecular mechanics (QM/MM) methodologies are limited to short sequences and short evolution time^{37–40}. This challenge calls for the development of coarse grained models with perturbative methods^{41–44}, model-system computational schemes⁴⁰, and phenomenological approaches^{31,35,36,45}. For example, the fluctuating nuclear environment of DNA can be described by adding noise terms to the static, purely electronic Hamiltonian. These fluctuations can be made spatially and temporally correlated, mimicking coordinated atomic motion^{25,46}.

With the goal to describe charge transport in 1-5 nm long DNA, identify central transport mechanisms, and pinpoint exceptionally good or poor DNA conductors, we recently performed extensive conductance calculations of metal-molecule-metal DNA junctions³¹. In our scheme, the electronic structure of the double helix is described with a coarse grained model^{47,48}, and the electrical conduction is calculated with a quantum scattering technique, the Landauer-Büttiker’s probe (LBP) method^{32,33}. This approach captures the impact of intra and inter-molecular motion (“thermal environment”) by introducing a tunable scattering parameter, γ_d , responsible for decohering the conducting charge and opening elastic and inelastic charge transport pathways^{34–36,49–59}. Physically, γ_d corresponds to a scattering rate constant, but here we report it with the dimension of energy.

The LBP method as applied to molecular junctions was detailed in several previous publications from our group, starting in Refs.^{56–58}, where general principles were explained. Applications to DNA junctions were discussed in Refs.^{34–36}. The code was presented in details in Ref.⁵⁹. LBP calculations performed in Ref.³¹ comprises the training set for the present study.

Briefly, the electronic Hamiltonian of dsDNA is modeled using a tight-binding ladder Hamiltonian with each site representing a particular base, see Fig. 1(a). The electronic energies of each site and the interstrand and intrastrand transition matrix elements t were generated by DFT calculations⁴⁷. The molecule-metal coupling strength $\gamma_{L,R}$ is taken in the range of 50-1000 meV, and the electronic temperature T_{el} at the metal leads is 5-300 K. Information on thermal-environmental effects are all incorporated within the parameter γ_d , taken in the range of 0-50 meV; the structure is rigid when $\gamma_d = 0$. Another tunable parameter is the position of the Fermi energy of the metals relative to molecular states. Since the HOMO of the guanine nucleotide lies the closest to the Fermi energy of gold electrodes, compared to the other nucleotides, we place the Fermi energy of the metals in resonance with the on-site energy of the guanine base. The LBP procedure involves the solution of an algebraic equation. It outputs the linear response (low voltage) electrical conductance G_{LBP} of the junction.

Calculations reported in Ref.³¹ were all-inclusive: For a given number of base pairs n , we considered all possible sequences satisfying the base-pairing rules and simulated the electrical conductance of each of these compounds using the LBP scheme. With this exhaustive approach, we discovered key principles governing charge transport in 3-7 bp DNA nanojunctions, which are 1-3 nm long. As an example, in Fig. 2 we display the conductance of dsDNA with $n = 5$ bp under increasing environmental effects. There are $N = 512$ such distinct sequences. As we discuss in Ref.³¹, we identify in this figure different families of molecules: good ($G = 1 - 0.01 G_0$), poor ($G < 10^{-10} G_0$), and intermediate conductors ($G = 10^{-2} - 10^{-6} G_0$). Here, $G_0 = e^2/h$ is the quantum of conductance per spin species, with the electron charge e and Planck’s constant

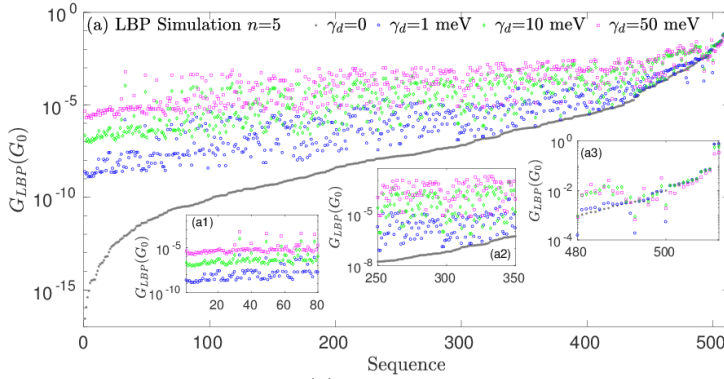
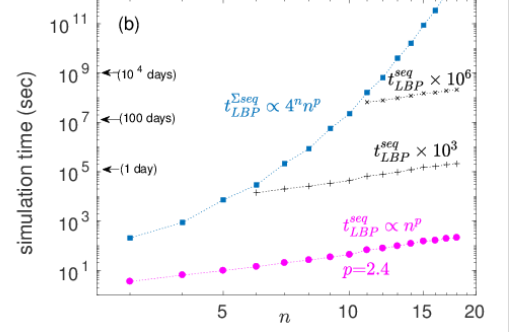


FIG. 2: LBP simulations. (a) Effect of the thermal environment on the conductance of sequences with five base pairs ($n = 5$, $N = 512$). Sequences are ordered by conductance values based on the case with environmental effects turned off. (b) Simulation times for a single sequence, t_{LBP}^{seq} (\circ), and for the whole ensemble of N molecules with n bp, $t_{LBP}^{\Sigma seq}$ (\square). We further provide LBP simulation times for a subset of 10^3 (+) and 10^6 (x) sequences with n bp. Simulation times are reported for $\gamma_d \neq 0$.



h. Good conductors (panel a3) are only mildly affected by the environment showing a quantum-wire properties; poor conductors (panel a1) enjoy a dramatic enhancement of their conductance, assisted by the environment, demonstrating a tunneling-to-hopping crossover. Nevertheless, the majority of the sequences cannot be categorized as tunneling/ohmic/ballistic conductors (panel a2), and their conductance under environmental effects largely depends on whether they have a local cluster of identical bases³¹.

The cost of LBP calculations rapidly increases with molecular length as we illustrate in Fig. 2(b). Here, we report the LBP computation cost for a single sequence of length n , t_{LBP}^{seq} , as well as the time it takes to generate G_{LBP} for the whole ensemble of N molecules with n base pairs, $t_{LBP}^{\Sigma seq}$. Simulations were performed on a quad core processor, Intel(R) Core™ i5-6400 CPU 2.70GHz. For example, the calculation of G_{LBP} for a single $n = 7$ sequence takes 20 sec. A complete scan of all 8,192 sequences with 7 bp takes about 2 days. Continuing in this fashion, calculating G_{LBP} for a single $n = 12$ sequence takes 1.3 min, thus computing 10^6 such values (a subgroup of the full space) requires about 900 days. A full sequence scan for $n = 12$ is impractical (see supplementary material for more information). All in all, it is clear that beyond $n = 8$, comprehensive calculations even with the highly simplified LBP method are impractical given the exponential growth of the sequence space. We next describe a ML approach that allows a rapid and accurate calculation of long range charge transport in DNA molecules.

C. Machine learning approach

Machine learning techniques are gaining much interest in the study of physical phenomena and in the exploration of the chemical space. For example, in condensed matter physics ML models detect, classify, and charac-

terize quantum phases and phase transitions in strongly correlated materials^{60,61}. In quantum chemistry, machine learning tools construct potential energy surfaces, identify reaction pathways^{62–64}, and predict excited state energies⁶⁵ and electronic correlation energies⁶⁶. Application of ML methods to studies of materials⁶⁷ and drug design⁶⁸, e.g. predicting drug-target binding affinities, can automate molecular discovery and synthesis⁶⁹.

Numerous applications of ML models are focused on materials with predictions made on the energy of the system: potential energy function, formation energy, electronic energy. In contrast, the potential of ML models to explore chemical dynamics, specifically probe the question of structure-dynamic, is still largely untouched. Some examples include Ref.⁷⁰, where a ML approach was used to predict the electrical conductance of disordered one-dimensional channels, and Refs.^{65,71}, in which excitation energy dynamics and transfer times in light harvesting systems were predicted with ML tools by considering a large dataset of model Hamiltonians.

1. Input representation: Descriptors for DNA charge transport

Our objective is to predict the electrical conductances of DNA junctions of arbitrary length based on the conductance of short DNA molecules of 3 to 7 bp. The input data representation (descriptor) should capture central features of DNA electrical transport. We opt here for a descriptor that does not rely on an energy function of the system or its Hamiltonian, unlike e.g. Ref.⁷¹. As such, the neural network (NN) can predict the conductance of long sequences—while trained on short chains. Since the input features used here are missing the fingerprints of the methodology (no model parameters), one could follow our steps, adopt the descriptors examined here, and train data generated from other methodologies besides the LBP method.

We devise and test different types of input features for DNA charge transport, which we identify as single (S), pair (P) and trio (T) descriptors. The smallest descriptor has four numbers as its input, and it only captures the composition of the sequence: We count the occurrences of each of the A,C,G, T nucleotides (in that order) in a single strand. For example, the sequence 5'AAATGG3' has an input descriptor [3021]. This descriptor is of type S, since it provides information on individual base pairs, as opposed to the P and T input features, which hand over information over local clusters.

The DNA ladder model involves nearest-neighbor intra- and inter-strand interactions. Indeed, an important aspect of DNA charge transport is that the transferred charge may be delocalized over several base pairs. It is therefore expected that besides composition, information over the ubiquity of pairs and threesomes (e.g., the appearance of the series GGG in a sequence) are paramount to charge transport characteristics of DNA. We therefore test P and T descriptors: The occurrence of pairs of nucleotides is described by an 4^2 -dimensional vector; the number of unique triplets is described by an 4^3 -dimensional vector. We list pairs and trios in alphabetical order: AAA, followed by AAC, AAG, AAT, ACA, etc. For example, the input descriptors S, P, and T of the sequence AAAAC are [4100], [310_{1×14}], and [210_{1×62}], respectively.

So far, the descriptors do not convey information on the fact that the examined molecule is positioned in a metal-molecule-metal configuration. As we demonstrated in Ref.³¹, the identity of the nucleotide connecting to the electrodes is important, particularly for short chains under coherent transport. Therefore, we expand the descriptors explained so far by adding two parameters that specify the bases, A, C, G, or T, connected to the electrodes.

Altogether, we organize six models with 4-, 6-, 16-, 18-, 64- and 66- dimensional descriptors, which we refer to as the NN-4, NN-6, NN-16,..., NN-66 models. In the next section we test these models. Generally, we observe that the NN-66 model provides the most accurate predictions.

2. Neural network architecture

We solve an input-output fitting problem with a shallow neural net consisting of a hidden and an output layer. The NN is trained using the Levenberg-Marquardt back propagation algorithm. The base-10 logarithm of the electrical conductance, obtained from the LBP method, is provided to the NN as the target value. We used the built-in MATLAB machine learning toolbox (trainlm) with a random assignment of the LBP data: 50% for training and 25% for validation and testing each. The algorithm adjusts the weights and biases from the initial guess to minimize the mean squared error, that is the averaged square error between the network outputs a_i and

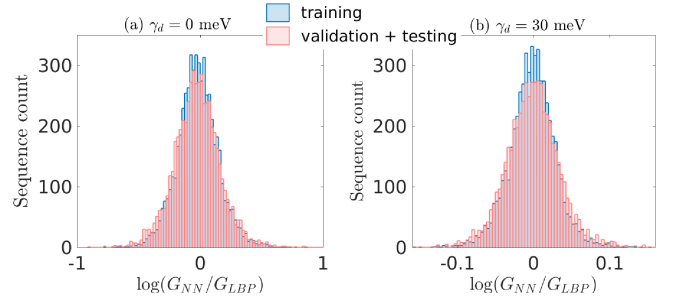


FIG. 3: Error distribution for training and validation+testing sets, (a) $\gamma_d = 0$, (b) $\gamma_d \neq 0$. Other parameters are $\gamma_{L,R} = 50$ meV, $T_{el} = 5$ K. We trained 10 networks with the NN-66 descriptor.

the targets t_i over a training set with K values. Since conductance values (in G_0) span up to 20 (!) orders of magnitude, we use base-10 logarithm of conductance as our model's input and output.

To train the NN, we collect 10,952 = 32 + 136 + 512 + 2080 + 8192 LBP calculations for DNA junctions with $n = 3$ to $n = 7$ bp. The model is trained on these sequences with a random 2:1:1 assignment for training, validation and testing sets.

We define deviations from the correct (LBP) value, $\Delta_i \equiv \log G_{NN}^{(i)} - \log G_{LBP}^{(i)}$. This measure is Gaussian-distributed with mean ≈ 0 . To characterize the model's accuracy and precision, we further define the mean absolute error (MAE) and the standard deviation (SD or σ) from the mean as $MAE \equiv \langle |\Delta| \rangle$, $\sigma^2 = \langle \Delta^2 \rangle$. The mean absolute error discloses how many orders of magnitude away from the correct value is a typical prediction; we use the modulus so as to capture absolute deviations (distance of values below and above) from the correct result. The standard deviation from the mean characterizes the width of the distribution (see e.g. Fig. 3).

We train several NN models, for a specific choice of $\gamma_{L,R}$, γ_d and T_{el} . Upon training, which takes under one second for the smallest descriptor and a little over 10 seconds for the largest one, the conductance values of millions of DNA sequences can be readily predicted, see Table I.

The weights and biases achieved upon training the NN may vary due to different initial guesses and the partition of the data set into training, validation, and test sets. As a result, neural networks that are trained on the same data set give somewhat different predictions. We find that an interpolation task (when the NN predicts the conductance of sequences of the same length as those trained on) is robust for our networks. However, when asking the NN to extrapolate to out-of-sample, longer sequences, variations between predictions may be substantial, by up to an order of magnitude when γ_d is small (1 meV). To address this issue, we train several (ten) neural networks on the same input data, and take the median of ten predictions as the model's prediction.

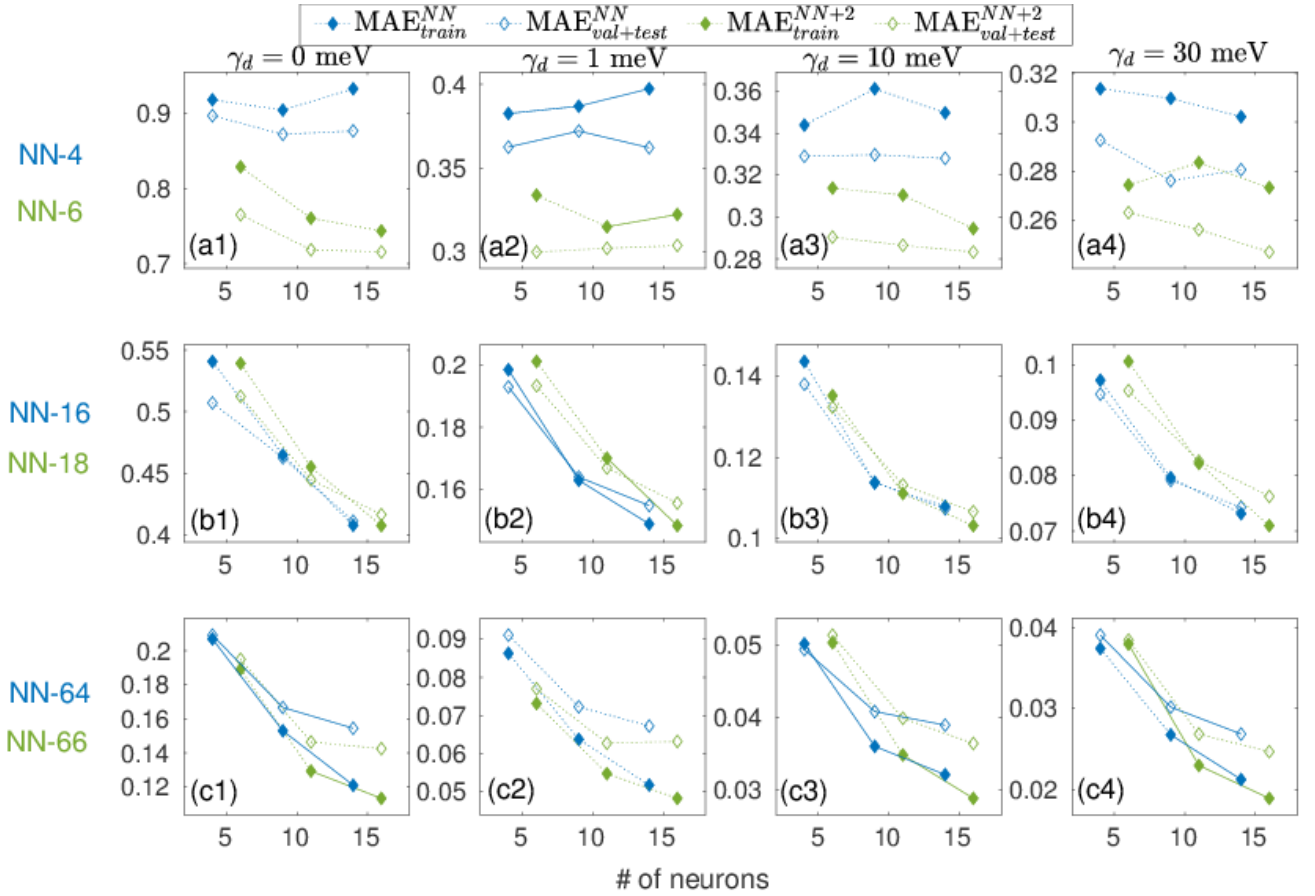


FIG. 4: Performance of the NN with 5, 10 and 15 neurons in its hidden layer (x-axis) for different descriptors (rows). The dataset includes all 10,952 sequences with $n = 3 - 7$ bp under different environmental effects $\gamma_d = 0, 1, 10, 30$ meV (columns). We display the MAE for both the training set (50% of the data) and validation+testing set (25% each). For clarity, results from different descriptors are shifted by ± 1 about 5, 10, and 15. Other parameters are $\gamma_{L,R} = 50$ meV, $T_{el} = 5$ K. Corresponding σ values are presented in the supplementary material file.

In Fig. 3, we display histograms of the training and validation-test errors Δ_i . Each prediction is the median of values from 10 neural networks with 10 neurons in their hidden layer. The 10 neural networks are trained on the same data set, but with different, random partitioning (2:1:1) into the training, validating and testing sets, respectively. We confirm that deviations of the ML prediction from the LBP values are distributed symmetrically around zero. It is important to note that the error at nonzero γ_d is significantly smaller than the rigid case, $\gamma_d = 0$. Similar results were obtained for other parameters.

In Fig. 4 we examine the performance of different descriptors, as well as the impact of the number of neurons in the hidden layer as we vary γ_d (columns). We show the MAE; results for the standard deviation are included in the supplementary material file. We examine six different descriptors. In each case we also test whether information over the connectivity (the base connected directly to the electrodes) is important for the quality of prediction. For example, $\text{MAE} = 0.2$ corresponds to

$G_{NN}/G_{LBP} = 10^{0.2}$, meaning that on average predictions are a factor of 1.6 from the correct one. $\text{MAE} = 0.02$ corresponds to $G_{NN}/G_{LBP} = 10^{0.02}$, thus predictions are highly accurate with an average 5% deviation from the correct value. For clarity, the number of neurons used for the two different descriptors, NN and NN+2, is displaced by ± 1 from the actual numbers of 5, 10, 15.

We make the following observations: (i) Scrolling down, it is clear that the largest, 66-dimensional descriptor manifests the best performance. This result is backed by physical knowledge over the role of small clusters of nucleotides in DNA charge transport. (ii) The information over the connectivity to the metal is important, particularly when γ_d is small, as evidenced by the significant narrowing of the MAE and the SD for all three descriptor types. (iii) The error is reduced as we increase γ_d . The fully coherent case ($\gamma_d = 0$) is the most challenging one for the ML model given the enormous range of conductance values. (iv) The number of neurons in the hidden layer is selected to ensure the best fit, but no over-fitting. We set on the optimal number of 10 neu-

rons. Larger networks do not substantially decrease the error for the validation and test sets. As one can see in Fig. 4 (for example panels b4 and c2), the performance of the 15-neuron networks is often not as good for the validation+testing as it is for the training set, indicating over-training. On the other hand, 5-neuron nets are mostly under-trained.

The ML framework could be improved in two ways. First, the training data was selected here at random from the full ensemble of molecules. However, the training set may be selected more carefully using e.g. principal component analysis as in Ref.⁷¹. This would allow us to (i) dismiss redundant information from sequences that are very similar in properties, and (ii) capture under-represented structures, such as homogeneous sequences. Second, the ML algorithm parameters such as the activation function, number of layers, regularization parameters, were not optimized here, besides the number of neurons in the hidden layer. Customizing the NN architectures could enhance the quality of predictions.

III. RESULTS

A. Interpolation and extrapolation predictions

We study the performance of the NN on different tasks. An interpolation prediction concerns training the NN on say 10,000 sequences of $n = 10$ bp, which is a subset of

the total 524,800 10-bp long sequences, then asking it to predict the conductance of another $n = 10$ sequence. An extrapolation task, in contrast, concerns training the NN on sequences that are $n = 3 - 7$ bp long, and using it to predict the conductance of longer molecules. Obviously, an extrapolation task is more economic since generating the dataset for long chains is costly, see the supplementary information file. We now show that our ML method can perform very well for both Interpolation and extrapolation tasks.

Beginning with an interpolation prediction, we exemplify the performance of the ML method for short sequences ($n = 5$) in Fig. 5. These results should be compared to LBP calculations of Fig. 2. We recall that LBP conductance of rigid molecules sets the ordering of sequences. Thus, the fact that in Fig. 5 the conductance of rigid molecules is not monotonic but it shows local fluctuations demonstrates errors in prediction, which can be an order of magnitude away from the correct LBP value for poor conductors. When environmental effects are included, predictions become quite accurate: Compare panels (a1)-(a3) in Fig. 5 to Fig. 2. Specifically, the NN reproduces the tunneling-to-hopping behavior for sequences 0 – 80, the quantum wire characteristics of good conductors (sequences 450+), and the behavior of sequences in between, see panel (a2).

The advantage of the ML framework is made clear in Table I. Predicting the conductance of 10^6 sequences with $n = 18$ bp takes several seconds (after training), which is 7 orders of magnitude faster than direct LBP calculations, see Fig. 2(b).

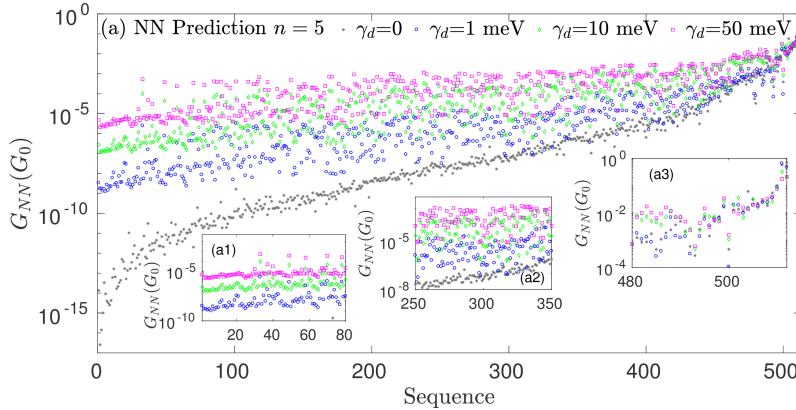


FIG. 5: ML prediction. Effect of the environment on the conductance of sequences with five base pairs ($n = 5$, $N=512$) as predicted by a machine learning algorithm with 10 neural networks trained on the same 50% of the data set, but subdivided randomly (and differently for 10 networks) between training (70%), validation (15%) and test (15%). Sequences are ordered according to LBP simulations at $\gamma_d = 0$.

procedure	time
building the dataset $n = 3 - 7$ (10,952 seq) $\gamma_d \neq 0$ $\gamma_d = 0$	2.3 days 20 mins
training 10 NN	2 min
prediction: 10^6 sequences with 10 NN, NN-6	1 sec
prediction: 10^6 sequences with 10 NN, NN-66	10 sec

TABLE I: Supervised training on a shallow NN using the Levenberg-Marquardt back-propagation algorithm.

The question of an extrapolation prediction (for out-of-set n), as opposed to an interpolation is examined in Fig. 6. Here, we display the conductance of $n = 8$ bp system

(total of $N = 32,896$ sequences) for two different values of γ_d , 1 and 10 meV. Each dot corresponds to a particular sequence. We begin in panel (a) with an all-inclusive

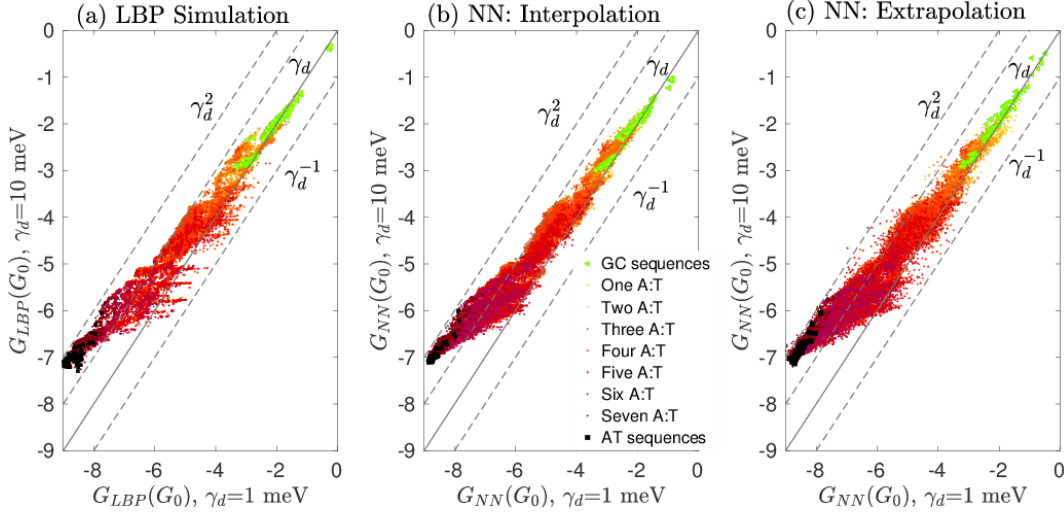


FIG. 6: Scaling of the conductance with environmental scattering rate γ_d for sequences with eight base pairs ($n = 8$, $N = 32,896$), (a) LBP calculations. Machine learning framework, with NN trained on 10,952 sequences of (b) length 8 and (c) length 3-7. Other parameters are $T_{el} = 300$ K, $\gamma_{L,R} = 50$ meV.

$\gamma_{L,R}$ (meV)	T_{el} (K)	$\gamma_d = 0$ (meV) MAE, σ	$\gamma_d = 1$ (meV) MAE, σ	$\gamma_d = 10$ (meV) MAE, σ	$\gamma_d = 30$ (meV) MAE, σ	$\gamma_d = 50$ (meV) MAE, σ
50	5	0.44, 0.63	0.17, 0.23	0.10, 0.14	0.071, 0.11	0.048, 0.075
50	300	0.71, 0.92	0.21, 0.30	0.085, 0.13	0.045, 0.081	0.028, 0.045
1000	5	0.50, 0.70	0.23, 0.31	0.16, 0.22	0.10, 0.14	0.080, 0.11
1000	300	0.70, 0.90	0.28, 0.38	0.13, 0.19	0.076, 0.12	0.56, 0.093

TABLE II: Mean absolute error and standard deviation of the mean error for extrapolation predictions G_{NN} for 8 bp long sequences.

LBP simulation. The best conductors are found on the diagonal, or slightly below it; they are either undisturbed or lightly negatively affected by thermal-incoherent scattering effects. Poor conductors follow the scaling $G \propto \gamma_d^2$. Most importantly, as reported in Ref.³¹, while we can identify ballistic (green) and ohmic (black) conductors, most molecules display an in-between behavior, $G \propto \gamma_d^\alpha$ with $0 \lesssim \alpha \lesssim 1$ at high electronic temperature. These sequences conduct via an *intermediate*, coherent-incoherent mechanism.

We use the ML model to reproduce these results. In panel (b), the dataset was generated for $n = 8$ bp molecules, and it includes the conductances of 10,952 sequences (out of the total of 32,896). In contrast, in panel (c) we train the NN on 10,952 short sequences with $n = 3 - 7$ bp. The three panels therefore present physical results, ML-interpolation, and ML-extrapolation predictions.

Overall, we find that both predictions are qualitatively correct. The ML algorithm performs very well for most of the sequences that display intermediate coherent-incoherent conduction. It also successfully identifies poor hopping and good ballistic conductors. Table II lists errors associated with the out-of-set (extrapolation) predictions.

B. Transport mechanisms

We use the NN model to extrapolate and predict conductance trends in families of DNA molecules with $n = 3 - 18$ base pairs. We emphasize that training is done on short sequences with $n = 3 - 7$ base pairs. The ML model is therefore expected to generalize results to out-of-sample sequences. We focus on three families of molecules:

(i) Sequences with an AT block, which display a tunneling-to-hopping crossover with increasing barrier length, as demonstrated experimentally in Ref.¹⁸ and computationally (with the LBP method) in Ref.³⁵. Our results are summarized in Fig. 7 with Table III listing examined sequences.

(ii) Alternating GC sequences, which display ohmic resistance. The electrical conductance of this family of molecules was recently measured in Ref.¹⁸, with calculations reported in Refs.^{35,36}. Our simulations of this family are summarized in Fig. 8 with Table IV listing the molecules.

(iii) Sequences with a uniform A block. The conductance of these homogeneous junctions was examined in Ref.³⁴, showing complex behavior: When environmental effects are weak ($\gamma_d \sim 0.001$ eV), we watch a transition

from deep-tunneling to resonant tunneling motion with increasing length. In contrast, when $\gamma_d = 10 - 50$ meV, we observe a crossover from tunneling to hopping conduction, similarly to case (i). Our results are summarized in Fig. 9 with Table V listing the molecules.

We now discuss our observations. Fig. 7 exemplifies the excellent ability of the NN model to predict transport mechanisms and provide accurate predictions for the conductance. It is significant to note that the conductance varies over 5 orders of magnitude. In panel (b) we display the ohmic behavior taking place when $\gamma_d = 30 - 50$ meV. The NN-66 model generally provides more accurate predictions than the NN-18 model, even when γ_d is large and charge transport is expected to be less delocalized over multiple sites.

Chains with alternating GC sequences are studied in Fig. 8. Experiments demonstrated that this system manifests an ohmic behavior with the resistance scaling as $R \propto n$, in accord with a site-to-site hopping conduction mechanism¹⁸. LBP calculations quantitatively reproduce these observations^{35,36}. We compare ML predictions to LBP simulations, showing mixed results. The NN model predicts an approximate linear enhancement of resistance with length when $\gamma_d = 10 - 30$ meV, but it misses this trend for smaller or larger values of γ_d .

Why are ML predictions here less accurate than in Fig. 8? First, one should appreciate that results of the ML model are mostly within $\pm 2M\Omega$ for $\gamma_d = 10 - 30$ meV. We can rationalize the reduced accuracy of the NN model as follows. Recall that the training set includes all different combinations of the four bases for sequences 3-7 bps. This ensemble of molecules realizes conductances ranging from $1G_0$ to $10^{-7}G_0$ for e.g. $\gamma_d = 10$ meV. In Fig. 8, however, we study a very specific subset of this ensemble, focusing on sequences that comprise a cluster of GC bps, with conductances that only mildly vary with distance. Predicting the behavior of a small, specific subset of molecules is therefore not trivial since they are not well represented in the training set. In principle, one could train the NN separately only on (short) GC molecules, to predict the behavior of long GC systems. However, for $n = 3 - 7$ there are only ~ 100 GC molecules, which is insufficient for a proper training and prediction. More practically, the training set could be carefully prepared

so as to ensure its diversity. All in all, we conclude that predicting the behavior of a specific subset of molecules out of the full ensemble is challenging, but that the NN model performs reasonable well for $\gamma_d = 10 - 30$ meV.

In Fig. 9, we study the $5'\text{-G(A)}_n\text{-G-3'}$ family with $n = 3 - 14$. Here, the bridge is uniform, thus it can support a resonant tunneling (band like) motion. This system displays three different transport regimes as we discussed in Ref.³⁴: (i) For short junctions, tunneling conduction dominates with a strong suppression of conductance with length. (ii) As long as the environment only lightly influences the system, $\gamma_d \lesssim 1$ meV, a resonant tunneling mechanism takes over deep tunneling in long enough chains. For a uniform bridge, resonant tunneling manifests itself with a distance independent conductance. (iii) In contrast, when γ_d is large, charge carriers hop from site to site, showing an ohmic trend for large n . Experimentally, it was recently demonstrated that the conductance of adenine-stacked RNA-DNA hybrids varied weakly with length³⁰, in what was termed as ‘coherence-corrected hopping’ mechanism²⁸.

We find that both NN-18 and NN-66 are quite successful in providing qualitatively (and even quantitatively) correct predictions. For short, $n < 5$, chains, the NN-18 input descriptor better performs than the NN-66, which is not surprising given that for such short systems a triplet information is redundant as most input entries are null. In contrast, for $n > 7$ the NN-66 is typically more successful than the pairwise model. However, in terms of transport mechanisms, similarly to Fig. 8, the ML model again is missing the ohmic characteristics: It captures the deep tunneling trend for short systems and the ballistic saturation for $n > 5$. However, it is not able to produce the ohmic trend for $\gamma_d \gtrsim 30$ meV.

We conclude that the NN model performed excellently in case (i) when molecules were composed quite evenly of the different bases, but its predictions were less accurate in the other two cases, when the molecules were predominantly composed of either GC or AT bp. However, even when missing the correct distance dependence, predictions were generally accurate (correct order of magnitude) for the NN-66 model. Ensuring that the training set includes unique, underrepresented sequences should improve predictions.

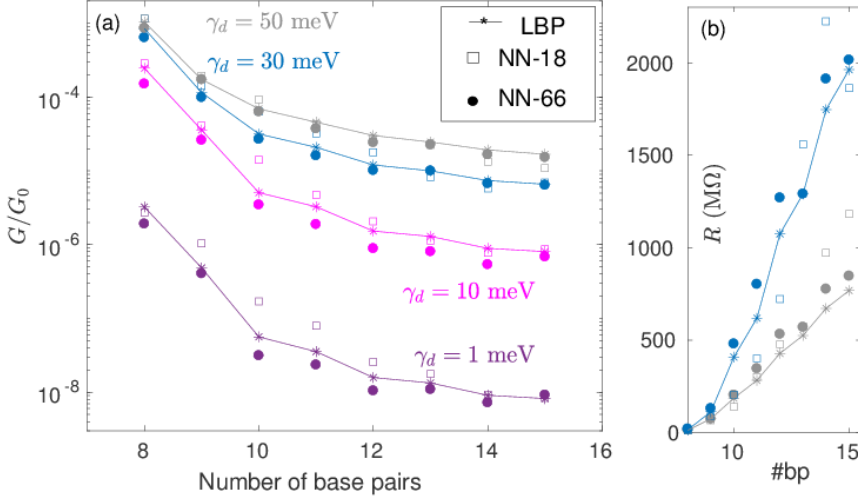


FIG. 7: Tunneling-to-hopping crossover in DNA junctions. (a) Conductance (log scale) of AT-block sequences (see Table III) as a function of the number of base pairs (#bp). (b) Highlighting the ohmic resistance at high γ_d . We compare LBP simulations (*) to NN-18 (\square) and NN-66 (\circ) predictions. Simulations were performed at $T_{el}=5$ K to attenuate the contribution of ballistic electrons. Other parameters are $\gamma_d=1, 10, 30, 50$ meV, $\gamma_{L,R}=50$ meV.

# bp	5'-seq-3'
8	ACGCAGCGT
9	ACGCATGCGT
10	ACGCATAGCGT
11	ACGC(AT) ₂ GCGT
12	ACGC(AT) ₂ AGCGT
13	ACGC(AT) ₃ GCGT
14	ACGC(AT) ₃ AGCGT
15	ACGC(AT) ₄ GCGT

TABLE III: AT-block sequences (seq) with 8-16 base pairs measured in Ref.¹⁸.

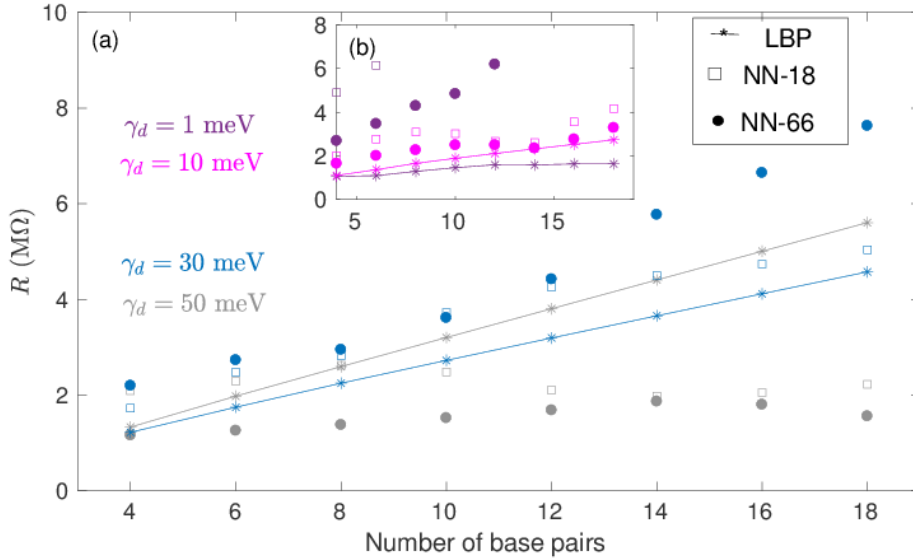


FIG. 8: (a)-(b) Electrical resistance of alternating GC-DNA sequences as a function of length, 5'-A(CG)_mT-3' with $m = 1 - 8$. LBP simulations (*), NN-18 (\square) and NN-66 (\circ) models. Other parameters are $\gamma_d=1, 10, 30, 50$ meV, $T_{el} = 300$ K, $\gamma_{L,R}=50$ meV.

# bp	5'-A(CG) _m T-3'
4	ACGT
6	A(CG) ₂ T
8	A(CG) ₃ T
10	A(CG) ₄ T
12	A(CG) ₅ T
14	A(CG) ₆ T
16	A(CG) ₇ T
18	A(CG) ₈ T

TABLE IV: Alternating GC-sequences measured in Ref.¹⁸ with calculations reported in Fig. 8.

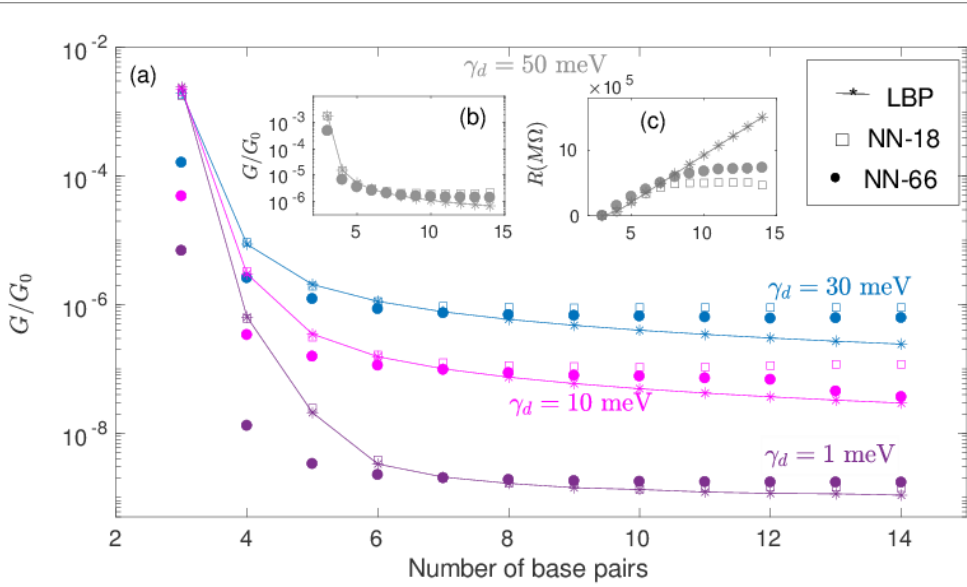


FIG. 9: Electrical conductance of sequences with an A block, $5'\text{-G(A)}_m\text{G-3}'$, $m = 1 - 12$. as a function of number of bp. We compare the NN-18 (\square) and NN-66 (\circ) predictions to LBP simulations ($*$). (b)-(c) Focusing on $\gamma_d = 50$ meV, we demonstrate that the NN models fail to capture the ohmic behavior, but yield results within the correct order of magnitude. Other parameters are $\gamma_d = 1, 10, 30, 50$ meV, $T_{el} = 300$ K, $\gamma_{L,R} = 50$ meV.

#bp	$5'\text{-G(A)}_n\text{G-3}'$ $n = 1 - 12$
3	GAG
4	$\text{G(A)}_2\text{G}$
5	$\text{G(A)}_3\text{G}$
6	$\text{G(A)}_4\text{G}$
7	$\text{G(A)}_5\text{G}$
...	...
14	$\text{G(A)}_{12}\text{G}$

TABLE V: Sequences with a uniform A block, studied previously in Ref.³⁴ with the LBP method, and examined with the NN models in Fig. 9.

IV. SUMMARY

We showed that a NN model could provide cheap predictions of molecular conductance of millions of long DNA nanojunctions with high accuracy. A central aspect of our work has been to test input features (descriptors) that do not rely on model parameters (such as the coarse grained Hamiltonian) and do not rightly announce on the base sequence. The developed descriptors provide information over molecular composition and the occurrence of local (2-3 bp) clusters. As such, the model is transferable to sequences of different length and to data generated from other microscopic methods.

The ML model was trained on the conductance of 3 to 7 bp sequences. It was tested against short molecules in this set, then used for predicting the behavior of $n = 8$ molecules. Moreover, we studied DNA sequences with 3-18 bp and demonstrated that the ML model could well reproduce the behavior of special sequence subsets: It traced the transition from fully coherent (deep tunneling) to ballistic (on-resonance) transfer for stacked A-sequences³⁴, and the tunneling to hopping crossover in sequences with an AT block³⁵. With mixed success, it recovered the hopping conduction in alternating GC-sequences³⁶. These results demonstrate that a ML method can provide a cheap assessment of quantum transport in DNA junction.

It would be interesting to generate datasets using other (relatively cheap) methods that perturbatively include electron-vibration interaction effects, see e.g.⁷²⁻⁷⁴ and explore the ability of the ML technique to reproduce other

transport mechanisms.

Before concluding, its worth recalling other types of measurements of charge migration in DNA besides the junction geometry, using electrochemistry^{3,75} or time-resolved spectroscopy^{13,14}. In analogy to our study, one could perform quantum dynamics and charge transfer calculations in short molecules using e.g. a quantum master equation approach, then generalize results to other sequences with an ML framework. Finally, the principles outlined in this work could be applied to other types of oligomers, biomolecules in particular, in an effort to explain and predict long-range, macroscopic electron transport behavior^{76,77}.

ACKNOWLEDGMENTS

D.S. acknowledges support from the Natural Sciences and Engineering Research Council Canada (NSERC) Discovery Grant and the Canada Research Chair program. The work of R.K. was supported by the Centre for Quantum Information and Quantum Control (CQIQC) summer fellowship at the University of Toronto and the University of Toronto Excellence Research Fund.

¹Chakraborty, T. *Charge Migration in DNA; Perspectives from Physics, Chemistry, and Biology*, Springer-Verlag: Berlin, 2007.

²Genereux, J. C.; Barton, J. K. Mechanisms for DNA Charge Transport. *Chemical Reviews* **2010**, *110*, 1642-1662.

³Arnold, A. R.; Grodick, M. A.; Barton J. K. DNA Charge Transport: From Chemical Principles to the Cell. *Cell Chemical Biology* **2016**, *23*, 183-197.

- ⁴McDonnell, K. J.; Chemler, J. A.; Bartels, P. L.; O'Brien, E.; Marvin, M. L.; Ortega, J.; Stern, R. H.; Raskin, L.; Li, G.-M.; Sherman, D. H.; Barton, J. K.; Gruber, S. B. A Human MUTYH Variant Linking Colonic Polyposis to Redox Degradation of the [4Fe4S]²⁺ Cluster. *Nat. Chem.* **2018**
- ⁵E. Stulz (Editor), G. H. Clever (Editor), *DNA in Supramolecular Chemistry and Nanotechnology*, Wiley, 2015.
- ⁶Drummond, T. G.; Hill, M. G.; Barton, J. K. Electrochemical DNA Sensors. *Nat. Biotechnol.* **2003**, *21*, 1192-1199.
- ⁷Yang, D.; Hartman, M. R.; Derrien, T. L.; Hamada, S.; An, D.; Yancey, K. G.; Cheng, R.; Määttä, M.; Luo, D. DNA Materials: Bridging Nanotechnology and Biotechnology. *Acc. Chem. Res.* **2014**, *47*, 1902-1911.
- ⁸Zhang, Y.; Zhang, W. B.; Liu, C.; Zhang, P.; Balaeff, A.; Beratan, D. N. DNA Charge Transport: Moving Beyond 1D. *Surf. Sci.* **2016**, *652*, 33-38.
- ⁹Beratan, D. N.; Naaman, R.; Waldeck, D. H. Charge and Spin Transport Through Nucleic Acids. *Current Opinion in Electrochemistry* **2017**, *4*, 175-181.
- ¹⁰Porath, D.; Lapidot, N.; Gomez-Herrero J. Charge Transport in DNA-Based Devices, in *Introducing Molecular Electronics*. Lect. Notes Phys. 680 (Springer-Verlag, Berlin Heidelberg 2005) Eds. G. Cuniberti, G. Fagas, and K. Richter, 411-444.
- ¹¹Xu, B.; Zhang, P.; Li, X.; Tao N. Direct Conductance Measurements of Single DNA Molecules in Aqueous Solution. *Nano Lett.* **2004**, *4*, 1105-1108.
- ¹²Dulic, D.; Tuukkanen, S.; Chung, C.-L.; Isambert, A.; Lavie, P.; Filoramo, A. Direct Conductance Measurements of Short Single DNA Molecules in Dry Conditions. *Nanotechnology* **2009**, *20*, 115502.
- ¹³Lewis, F. D.; Zhu, H.; Daublain, P.; Fiebig, T.; Raytchev, M.; Wang, Q.; Shafirovich, V. Crossover From Superexchange to Hopping as the Mechanism for Photoinduced Charge Transfer in DNA Hairpin Conjugates. *J. Am. Chem. Soc.* **2006**, *128*, 791-800.
- ¹⁴Harris, M. A.; Mishra, A. K.; Young, R. M.; Brown, K. E.; Wasielewski, M. R.; Lewis, F. D. Direct Observation of the Hole Carriers in DNA Photoinduced Charge Transport. *J. Am. Chem. Soc.* **2016**, *138*, (17), 5491-5494.
- ¹⁵Kelley S. O.; Barton, J. K. Electron Transfer Between Bases in Double Helical DNA. *Science* **1999**, *283*, 375.
- ¹⁶Giese, B.; Amaudrut, J.; Köhler, A.-K.; Spormann, M. Wessely, S. Direct Observation of Hole Transfer Through DNA by Hopping Between Adenine Bases and by Tunnelling. *Nature* **2001**, *412*, 318-320.
- ¹⁷Wohlgamuth, C. H.; McWilliams, M. A.; Slinker, J. D. DNA as a Molecular Wire: Distance and Sequence Dependence. *Anal. Chem.* **2013**, *85*, 8634-8640.
- ¹⁸Li, Y.; Xiang, L.; Palma, J.; Asai, Y.; Tao, N. Thermoelectric Effect and its Dependence on Molecular Length and Sequence in Single DNA Molecules. *Nature Comm.* **2016**, *7*, 11294.
- ¹⁹Beall, E.; Ulku, S.; Liu, C.; Wierzbinski, Zhang, Y.; Bae, Y.; Zhang, P.; Achim, C.; Beratan, D. N.; Waldeck, D. H. Effects of the Backbone and Chemical Linker on the Molecular Conductance of Nucleic Acid Duplexes. *J. Am. Chem. Soc.* **2017**, *139*, 6726-6735.
- ²⁰Xuan, S.; Meng, Z.; Wu, X.; Wong, J.-R.; Devi, G.; Yeow, E. K. L.; Shao, F. Efficient DNA-Mediated Electron Transport in Ionic Liquids. *ACS Sustainable Chemistry and Engineering* **2016**, *4*, 6703-6711.
- ²¹Artes, J. M.; Li, Y.; Qi, J.; Anantram, M.P.; Hihath, J. Conformational Gating of DNA Conductance. *Nature Comm.* **2015**, *6*, 8870.
- ²²Renaud, N.; Harris M. A.; Singh, P. N.; Berlin, Y. A.; Ratner, M. A.; Wasielewski, M. R.; Lewis, F. D.; Grozema F. C. Deep-Hole Transfer Leads to Ultrafast Charge Migration in DNA Hairpins. *Nat. Chem.* **2016**, *8*, 1015-1021.
- ²³Jimenez-Monroy, K. L.; Renaud, N.; Drijckoning, J.; Cortens, D.; Schouteden, K.; van Haesendonck C.; Guedens, W. J.; Manca, J. V.; Siebbeles, L. D. A.; Grozema, F. C.; Wagner, P. H. High Electronic Conductance through Double-Helix DNA Molecules with Fullerene Anchoring Groups. *J. Phys. Chem. A* **2017**, *121*, 1182-1188.
- ²⁴Xiang, L.; Palma, J. L.; Li, Y.; Mujica, V.; Ratner, M. A.; Tao, N. Gate-Controlled Conductance Switching in DNA. *Nature Comm.* **2017**, *8*, 14471.
- ²⁵Zhang, Y.; Liu, C.; Balaeff, A.; Skourtis, S. S.; Beratan, D. N. Biological Charge Transfer via Flickering Resonance. *Proc. Natl. Acad. Sci. U.S.A* **2014**, *111*, 10049-10054.
- ²⁶Slinker, J. D.; Muren, N. B.; Renfrew, S. E.; Barton, J. K. DNA Charge Transport Over 34 nm. *Nat. Chem.* **2011**, *3*, 228-233.
- ²⁷Renaud, N.; Berlin, Y. A.; Lewis, F. D.; Ratner, M. A. Between Superexchange and Hopping: An Intermediate Charge-Transfer Mechanism in Poly(A)-Poly(T) DNA Hairpins. *J. Am. Chem. Soc.* **2013**, *135*, 3953-3963.
- ²⁸Xiang, L.; Palma, J. L.; Bruot, C.; Mujica, V.; Ratner, M. A.; Tao, N. Intermediate Tunneling-Hopping Regime in DNA Charge Transport. *Nat. Chem.* **2015**, *7*, 221-226.
- ²⁹Liu, C.; Xiang, L.; Zhang, Y.; Zhang, P.; Beratan, D. N.; Li, Y.; Tao, N. Engineering Nanometer-Scale Coherence in soft Matter. *Nat. Chem.* **2016**, *8*, 941-945.
- ³⁰Li, Y.; Artes, J. M.; Hihath, J. Long-Range Charge Transport in Adenine-Stacked RNA:DNA Hybrids, *Small* **2016**, *12*, 432-437.
- ³¹Korol R.; Segal, D. From Exhaustive Simulations to Key Principles in DNA Nanoelectronics. *J. Phys. Chem. C* **2018**, *122*, 4206-4216.
- ³²Büttiker, M. Small Normal-Metal Loop Coupled to an Electron Reservoir. *Phys. Rev. B* **1985**, *32*, 1846-1849.
- ³³Büttiker, M. Role of Quantum Coherence in Series Resistors. *Phys. Rev. B* **1986**, *33*, 3020-3026.
- ³⁴Kim H.; Segal, D. Controlling Charge Transport Mechanisms in Molecular Junctions: Distilling Thermally-Induced Hopping from Coherent-Resonant Conduction. *J. Chem. Phys.* **2017**, *146*, 164.
- ³⁵Korol, R.; Kilgour, M.; Segal, D. Thermopower in Molecular Junctions: Tunneling to Hopping Crossover in DNA. *J. Chem. Phys.* **2016**, *145*, 224702.
- ³⁶Kim, H.; Kilgour, M.; Segal, D. Intermediate Coherent-Incoherent Charge Transport: DNA as a Case Study. *J. Phys. Chem. C* **2016**, *120*, 23951-23962.
- ³⁷Gutierrez, R.; Caetano, R.; Woiczikowski, P. B.; Kubar, T.; Elstner, M.; Cuniberti, G. Structural Fluctuations and Quantum Transport through DNA Molecular Wires: a Combined Molecular Dynamics and Model Hamiltonian Approach. *New J. Phys.* **2010**, *12*, 023022.
- ³⁸Kubar, T.; Kleinekathöfer, U.; Elstner, M. Solvent Fluctuations Drive the Hole Transfer in DNA: A Mixed Quantum-Classical Study. *J. Phys. Chem. B* **2009**, *113*, 13107-13117.
- ³⁹Kubar, T.; Elstner, M.; Popescu, B. Kleinekathöfer, U. Polaron Effects on Charge Transport through Molecular Wires: A Multi-scale Approach. *J. Chem. Theory and Comp.* **2017**, *13*, 286-296.
- ⁴⁰Wolter, M.; Elstner, M.; Kleinekathöfer, U.; Kubar, T. Microsecond Simulation of Electron Transfer in DNA: Bottom-Up Parametrization of an Efficient Electron Transfer Model Based on Atomistic Details. *J. Phys. Chem. B* **2017**, *121*, 529-549.
- ⁴¹Gutierrez, R.; Mohapatra, S.; Cohen, H.; Porath, D.; Cuniberti, G. Inelastic Quantum Transport in a Ladder Model: Implications for DNA Conduction and Comparison to Experiments on Suspended DNA Oligomers. *Phys. Rev. B* **2006**, *74*, 235105.
- ⁴²Wang, X. F.; Chakraborty, T. Charge Transfer via a Two-Strand Superexchange Bridge in DNA. *Phys. Rev. Lett.* **2006**, *97*, 106602.
- ⁴³Brisker-Klaiman D.; Peskin, U. Ballistic Charge Transport Through Bio-Molecules in Dissipative Environment. *Phys. Chem. Chem. Phys.* **2012**, *14*, 13835-13840.
- ⁴⁴Blancafort, L.; Voityuk, A. A. Thermally Induced Hopping Model for Long-Range Triplet Excitation Energy Transfer in DNA. *Phys. Chem. Chem. Phys.* **2018**, *20*, 4997-5000.
- ⁴⁵Karasch, P.; Ryndyk, D. A.; Frauenheim, T. Vibronic Dephasing Model for Coherent-to-Incoherent Crossover in DNA. *Phys. Rev.*

- B* **2018**, *97*, 195401.
- ⁴⁶Liu, C.; Beratan, D. N.; Zhang, P. Charge- Grained Theory of Biological Charge Transfer with Spatially and Temporally Correlated Noise. *J. Phys. Chem. B* **2016**, *120*, 3624-3633.
 - ⁴⁷Senthilkumar, K.; Grozema, F. C.; Guerra, C. F.; Bickelhaupt, F. M.; Lewis, F. D.; Berlin, Y. A.; Ratner, M. A.; Siebbeles, L. D. A. Absolute Rates of Hole Transfer in DNA. *J. Am. Chem. Soc.* **2005**, *127*, 14894-14903.
 - ⁴⁸Zilly, M.; Ujsaghy, O.; Wolf, D. E. Conductance of DNA Molecules: Effects of Decoherence and Bonding. *Phys. Rev. B* **2010**, *82*, 125125.
 - ⁴⁹D'Amato J. L.; Pastawski, H. M. Conductance of a Disordered Linear Chain Including Inelastic Scattering Events. *Phys. Rev. B* **1990**, *41*, 7411.
 - ⁵⁰Pastawski, H. M. Classical and Quantum Transport from Generalized Landauer-Büttiker Equations. II. Time-Dependent Resonant Tunneling. *Phys. Rev. B* **1992**, *46*, 4053.
 - ⁵¹Roy D.; Dhar, A. Electron Transport in a One Dimensional Conductor with Inelastic Scattering by Self-Consistent Reservoirs. *Phys. Rev. B* **2007**, *75*, 195110.
 - ⁵²Nozaki, D.; Girard, Y.; Yoshizawa, K. Theoretical Study of Long-Ranged Electron Transport in Molecular Junctions. *J. Phys. Chem. C* **2008**, *112*, 17408-17415.
 - ⁵³Qi, J.; Edirisinghe, N.; Rabbani, M. G.; Anantram, M. Unified Model for Conductance Through DNA with the Landauer-Büttiker Formalism. *Phys. Rev. B* **2013**, *87*, 085404.
 - ⁵⁴Chen, S. G.; Zhang, Y.; Koo, S. K.; Tian, H.; Yam, C. Y.; Chen, G. H.; Ratner, M. A. Interference and Molecular Transport-A Dynamical View: Time-Dependent Analysis of Disubstituted Benzenes. *J. Phys. Chem. Lett.* **2014**, *5*, 2748-2752.
 - ⁵⁵Venkataramani, R.; Wierzbinski, E.; Waldeck, D. H.; Beratan, D. N. Breaking the Simple Proportionality Between Molecular Conductances and Charge Transfer Rates. *Faraday Discuss.* **2014**, *174*, 57-78.
 - ⁵⁶Kilgour, M.; Segal, D. Charge Transport in Molecular Junctions: From Tunneling to Hopping with the Probe Technique. *J. Chem. Phys.* **2015**, *143*, 024111.
 - ⁵⁷Kilgour M.; Segal, D. Tunneling Diodes under Environmental Effects. *J. Phys. Chem. C* **2015**, *119*, 25291-25297.
 - ⁵⁸Kilgour M.; Segal, D. Inelastic Effects in Molecular Transport Junctions: The Probe Technique at High Bias. *J. Chem. Phys.* **2016**, *144*, 124107.
 - ⁵⁹Korol, R.; Kilgour, M.; Segal, D. ProbeZT: Simulation of Transport Coefficients of Molecular Electronic Junctions under Environmental Effects Using Büttiker's Probes. *Comp. Phys. Comm.* **2018**, *224*, 396-404.
 - ⁶⁰Carrasquilla, J.; Melko, R. G. Machine Learning Phases of Matter. *Nature Phys.* **2017**, *13*, 431-434.
 - ⁶¹Ch'ng, K.; Carrasquilla, J.; Melko, R. G.; Khatami, E. Machine Learning Phases of Strongly Correlated Fermions. *Phys. Rev. X* **2017**, *7*, 031038.
 - ⁶²Jiang, B.; Li, J.; Guo, H. Potential Energy Surfaces from High Fidelity Fitting of ab initio Points: the Permutation Invariant Polynomial - Neural Network Approach. *Int. Rev. Phys. Chem.* **2016**, *35*, 479-506.
 - ⁶³Smith, J. S.; Isayev, O.; Roitberg, A. E. ANI-1: an Extensible Neural Network Potential with DFT Accuracy at Force Field Computational Cost. *Chem. Sci.* **2017**, *8*, 3192-3203.
 - ⁶⁴Smith, J. S.; Nebgen, B.; Lubbers, N.; Isayev, O.; Roitberg, A. E. Less is More: Sampling Chemical Space with Active Learning. *J. Chem. Phys.* **2018**, *148*, 241733.
 - ⁶⁵Häse, F.; Valleau, S.; Pyzer-Knapp, E.; Aspuru-Guzik, A. Machine Learning Exciton Dynamics. *Chem. Sci.* **2016**, *7*, 5139-5147.
 - ⁶⁶Welborn, M.; Cheng, L.; Miller III, T. F. Transferability in Machine Learning for Electronic Structure via the Molecular Orbital Basis. *J. Chem. Theory Comput.* **2018**, *14*, 4772-4779.
 - ⁶⁷Faber, F. A.; Lindmaa, A.; von Lilienfeld, O. A.; Armiento, R.; Machine Learning Energies of 2 Million Elpasolite Crystals. *Phys. Rev. Lett.* **2016**, *117*, 135502.
 - ⁶⁸Chen, H.; Engkvist, O.; Wang, Y.; Olivecrona, M. Blaschke, T. The Rise of Deep Learning in Drug Discovery. *Drug Discovery Today* **2018**, *23*, 1241-1250.
 - ⁶⁹Ahneman, D. T.; Estrada, J. G.; Lin, S.; Dreher, S. D.; Doyle, A. G. Predicting Reaction Performance in C-N Cross-Coupling Using Machine Learning. *Science* **2018**, *360*, 186-190.
 - ⁷⁰Lopez-Bezanilla, von Lilienfeld, O. A. Modeling Electronic Quantum Transport with Machine Learning. *Phys. Rev. B* **2014**, *89*, 235411.
 - ⁷¹Häse, F.; Kreisbeck, C.; Aspuru-Guzik, A. Machine Learning for Quantum Dynamics: Deep Learning of Excitation Energy Transfer Properties. *Chem. Sci.* **2017**, *8*, 8419-8426.
 - ⁷²Sowa, J.K.; Mol, J. A.; Briggs, G. A. D.; Gauger, E. M. Beyond Marcus Theory and the Landauer-Büttiker Approach in Molecular Junctions: A Unified Framework, *J. Chem. Phys.* **2018**, *149*, 154112.
 - ⁷³Levine, A. D.; Iv, M.; Peskin, U. Length-Independent Transport Rates in Biomolecules by Quantum Mechanical Unfurling. *Chem. Sci.* **2016**, *7*, 1535-1542.
 - ⁷⁴Levine, A. D.; Peskin, U. Formulation of Long-Range Transport Rates through Molecular Bridges: From Unfurling to Hopping. *J. Phys. Chem. Lett.* **2018**, *9*, 4139-4145.
 - ⁷⁵Beratan, D. N.; Naaman, R.; Waldeck, D. H. Charge and Spin Transport through Nucleic Acids. *Current Opinion in Electrochemistry* **2017**, *4*, 175-181.
 - ⁷⁶Ing, N. L.; El-Nagggar, M. Y. Hochbaum, A. I. Going the Distance: Long-Range Conductivity in Protein and Peptide Bioelectronic Materials. *J. Phys. Chem. B* **2018**, *122*, 10403-10423.
 - ⁷⁷Amdursky, N.; Glowacki, E. Meredith, P. Macroscale Biomolecular Electronics and Ionics. *Adv. Mater.* **2018**, 1802221.